

Nematic phases and elasto-resistivity from a multi-orbital strange metal

Andrew Hardy,^{1,*} Arijit Haldar,^{1,†} and Arun Paramekanti^{1,‡}

¹*Department of Physics, University of Toronto, 60 St. George Street, Toronto, ON, M5S 1A7 Canada*
(Dated: March 23, 2022)

We propose and study a two-orbital lattice extension of the Sachdev-Ye-Kitaev model in the large- N limit. The phase diagram of this model features a high temperature isotropic strange metal which undergoes a first-order thermal transition into a nematic insulator or a continuous thermal transition into nematic metal phase, separated by a tunable tricritical point. These phases arise from spontaneous partial orbital polarization of the multi-orbital non-Fermi liquid. We explore the spectral and transport properties of this model, including the d.c. elasto-resistivity, which exhibits a peak near the nematic transition, as well as the nonzero frequency elastoconductivity. Our work offers a useful perspective on nematic phases and transport in correlated multi-orbital systems.

Introduction. – The interplay of non-Fermi liquid physics (nFL) with broken symmetry states of matter is a rich field of research in correlated electron systems. One approach to this physics is to study metallic quantum critical points (QCPs) where fluctuations associated with the onset of symmetry breaking can destroy quasiparticles on the Fermi surface [1–7]. An equally important exploration is to ask how nFLs, also known as strange metals (SM), with a large density of low energy electronic excitations but no well-defined electronic quasiparticles, become unstable to diverse broken symmetry phases as we lower temperature [8–13]. Understanding these issues is of enormous interest for ongoing experiments on a wide range of quantum materials.

The electron nematic, a quantum liquid crystal, is a broken symmetry phase associated with the loss of lattice rotational symmetry. Nematicity and non-Fermi liquid physics have been explored in a host of correlated quantum materials including Moiré crystals such as twisted bilayer graphene with flat bands [14–16], iron pnictide and selenide systems [17–25], doped cuprates [26–28], the bilayer strontium ruthenates [29–34], and quantum Hall fluids [35–40]. Nematic quantum criticality is also of great interest since it impacts electrons on the entire Fermi surface. Quantum Monte Carlo simulations of sign-problem free models show signatures of non-Fermi liquid properties and an emergent superconducting dome near the nematic QCP [12, 41].

On the experimental front, a particularly useful tool to detect nematic fluctuations and symmetry breaking is elasto-resistivity. This measures the impact of uniaxial strain on the resistive anisotropy, providing a transport probe of the nematic susceptibility [42–45]. Given the diversity of systems exhibiting nematic symmetry breaking, it is important to understand elasto-resistivity in strongly correlated systems [46], including extensions to multi-orbital and multi-band non-Fermi liquids which is of relevance to FeSe, Sr₃Ru₂O₇, and Moiré crystals.

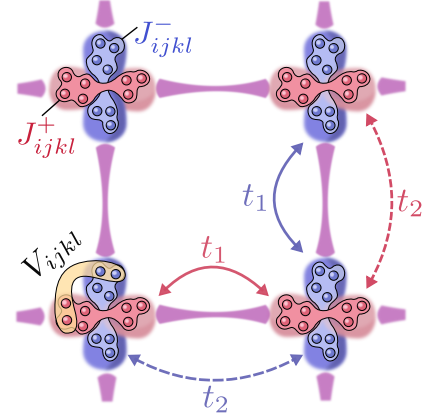


FIG. 1. The two-orbital SYK model: Two independent SYK ‘dots’ representing orbitals (denoted as red (+) and blue-filled circles (-)) are placed at each site \mathbf{r} of a square lattice. The orbitals at any given site have an SYK-type self-interaction (denoted $J_{ijkl}^+(\mathbf{r})$ and $J_{ijkl}^-(\mathbf{r})$) and an inter-orbital SYK-type interaction ($V_{ijkl}(\mathbf{r})$). Orbitals of the same type on neighboring lattice sites are connected via anisotropic hoppings with an ‘easy’ axis ($t_1 = t + \delta t$) and a ‘hard’ axis ($t_2 = t - \delta t$). The easy axis for the ‘+’ (red) orbitals point along the horizontal direction, while the easy axis for the ‘-’ (blue) orbitals point along the vertical direction.

Recently the theoretical study of nFLs has also seen significant progress. Starting with the formulation of the Sachdev-Ye-Kitaev (SYK) model [47–50] as a solvable example of nFL on a quantum dot, the field has grown to include several illuminating generalizations [51–59]. In this context, lattice extensions of the SYK model are particularly interesting since they provide a controlled route to accessing several phenomena, including lattice nFLs [60, 61], FL to nFL crossover [62–64], metal-insulator transition [65], heavy fermion physics [66], and critical Fermi surfaces [64, 67]. However, the question of how nematicity impacts a high-temperature nFL phase of an SYK lattice remains unexplored. In particular, is it possible to formulate a theoretically-solvable microscopic model with interactions that spontaneously manifest a nematic phase in the thermodynamic limit?

In this Letter, we address this question and other is-

* andrew.hardy@mail.utoronto.ca

† arijit.haldar@utoronto.ca

‡ arun.paramekanti@utoronto.ca

sues highlighted above by constructing a two-orbital extension of a lattice SYK model schematically depicted in Fig. 1. The two orbitals may be viewed as representing, for instance, d_{xz} and d_{yz} orbitals, each with a preferred hopping anisotropy, which play a role in many quantum materials. The underlying symmetry of this system is a C_4 lattice rotation followed by the exchange of the two orbitals. Orbital polarization breaks this symmetry down to C_2 , resulting in an Ising nematic. We study the complete phase diagram, thermodynamics, spectral functions, and transport, for this model in the large- N limit. We show that this model exhibits a non-Fermi liquid phase at high temperature, which gives way to a nematic insulator or a nematic metal upon cooling. Depending on parameters, this thermal transition is first-order or continuous, with a tunable tricritical point. We examine the transport properties of this model, including the impact of uniaxial strain which breaks orbital degeneracy. We find that uniaxial strain leads to a peak in the d.c. elasto-resistivity anisotropy in the vicinity of the isotropic-to-nematic transition. We also discuss the frequency dependent elastoconductivity.

Two-orbital SYK lattice model. – The SYK model represents a single-site ‘dot’ with N fermionic modes having random all-to-all interactions which is exactly solvable when $N \rightarrow \infty$. We generalize the SYK model to a square lattice with each site having two ‘SYK dots’, representing two orbitals, and each orbital accommodating N fermionic modes. Modes in the two orbitals hop anisotropically on the lattice, with a preferred direction as shown in Fig. 1: modes in orbital $s = “+”$ (red) hop along the \hat{x} and \hat{y} directions with respective amplitudes $t_1 = t + \delta t$ and $t_2 = t - \delta t$, with $\delta t > 0$, and vice versa for

modes in orbital $s = “-”$ (blue). The kinetic energy is

$$H_{\text{kin}} = \sum_{\mathbf{k}, s, i} \varepsilon_s(\mathbf{k}) c_{\mathbf{k}, s, i}^\dagger c_{\mathbf{k}, s, i} \quad (1)$$

where \mathbf{k} is the momentum, $s = \pm$ is the orbital, $i = 1 \dots N$ denote modes in each orbital, and the dispersion $\varepsilon_\pm(\mathbf{k}) = -2t(\cos k_x + \cos k_y) \mp 2\delta t(\cos k_x - \cos k_y)$.

The interactions take on the SYK form, with two-body intra-orbital and inter-orbital pair-hopping terms:

$$H_{\text{SYK}}^{\text{intra}} = \sum_{\mathbf{r}, s, (ijkl)} J_{ijkl}^{(s)}(\mathbf{r}) c_{\mathbf{r}, s, i}^\dagger c_{\mathbf{r}, s, j}^\dagger c_{\mathbf{r}, s, k} c_{\mathbf{r}, s, l} \quad (2)$$

$$H_{\text{SYK}}^{\text{inter}} = \sum_{\mathbf{r}, (ijkl)} V_{ijkl}(\mathbf{r}) c_{\mathbf{r}, +, i}^\dagger c_{\mathbf{r}, +, j}^\dagger c_{\mathbf{r}, -, k} c_{\mathbf{r}, -, l} + \text{H.c.} \quad (3)$$

where ‘‘H.c.’’ denotes Hermitian conjugate. The couplings $J_{ijkl}^{(s)}(\mathbf{r})$, $V_{ijkl}(\mathbf{r})$ are uncorrelated random complex numbers having Gaussian distributions with *zero*-mean, and satisfy $\langle\langle J_{ijkl}^{(s)}(\mathbf{r})^* J_{ijkl}^{(s')}(\mathbf{r}') \rangle\rangle = \delta_{ss'} \delta_{\mathbf{r}\mathbf{r}'} J^2 / (2N)^3$ and $\langle\langle V_{ijkl}(\mathbf{r})^* V_{ijkl}(\mathbf{r}') \rangle\rangle = \delta_{\mathbf{r}\mathbf{r}'} V^2 / (2N)^3$, respectively. Here $\langle\langle \dots \rangle\rangle$ denotes the average over all disorder realizations and $J^2 / (2N)^3$ and $V^2 / (2N)^3$ sets the variance. The couplings are properly antisymmetrized to obey $J_{ijkl}^{(s)} = -J_{jikl}^{(s)} = -J_{ijlk}^{(s)}$, and a similar condition holds for V_{ijkl} as well. To solve for the phase diagram of this model, we go to a path integral formulation and average over disorder via the replica trick. We use a replica diagonal ansatz for the local frequency dependent self-energy and lattice Green functions (see Supplemental Material for details); in the large- N limit, these quantities are also orbital-diagonal. The resulting free energy functional $\Omega = \sum_s \Omega_s$, with

$$\begin{aligned} \Omega_s = & -\frac{1}{\beta} \sum_{i\omega_n} \int d\varepsilon g(\varepsilon) \ln \left[\frac{i\omega_n + \mu - \varepsilon - \Sigma_s(i\omega_n)}{i\omega_n + \mu} \right] + \int_0^\beta d\tau \Sigma_s(\tau) G_s(\beta - \tau) \\ & - \frac{J^2}{4} \int_0^\beta d\tau G_s^2(-\tau) G_s^2(\tau) - \frac{V^2}{4} \int_0^\beta d\tau G_s^2(-\tau) G_{-s}^2(\tau) - \frac{1}{\beta} \ln(1 + e^{\beta\mu}), \end{aligned} \quad (4)$$

where $g(\varepsilon)$ is the lattice density of states, μ is the chemical potential, and τ , $\omega_n = (2n+1)\pi/\beta$ represent imaginary time and fermionic Matsubara frequencies, respectively, with $\beta = T^{-1}$ where T represents temperature. The imaginary-time Green’s function $G_s(\tau)$ satisfy the boundary condition $G_s(-\tau) = -G_s(\beta - \tau)$, and so does the imaginary-time self energy $\Sigma_s(\tau)$. Setting $\delta\Omega/\delta G_s(\tau) = 0$ and $\delta\Omega/\delta \Sigma_s(i\omega_n) = 0$ leads to

$$\Sigma_s(\tau) = -J^2 G_s^2(\tau) G_s(-\tau) - V^2 G_s^2(\tau) G_{-s}(-\tau) \quad (5)$$

$$G_s(i\omega_n) = \int d\varepsilon g(\varepsilon) [i\omega_n + \mu - \varepsilon - \Sigma_s(i\omega_n)]^{-1} \quad (6)$$

which we solve self-consistently (see Ref. [61] and Sup-

plemental Material for details). The solution is used to compute the equilibrium free energy and thermodynamic properties using Eq. 4.

Phase diagram. – We begin by discussing the nematic order which appears as a symmetry breaking solution to the above equations with $\Sigma_+ \neq \Sigma_-$. This phase may be viewed as a lattice generalization of the flavor-imbalanced phase of a two-flavor SYK model [52, 68]. As shown in Fig. 2(a), for $V = J = 1$, the nematic phase is separated from an isotropic SM by a first-order nematic transition at small hopping amplitude t . Increasing t , we encounter a tricritical point beyond which the thermal-nematic transition becomes second order; the

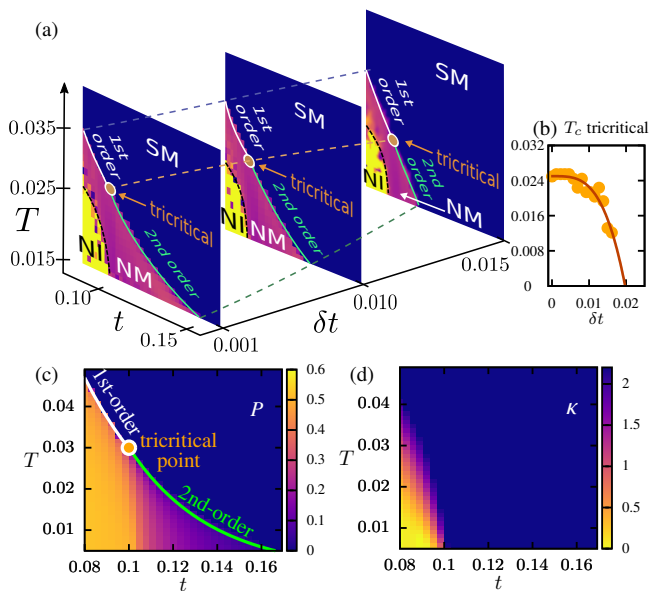


FIG. 2. (a) Phase diagram in terms of temperature (T), hopping (t), and hopping anisotropy δt , showing an isotropic strange metal (SM), a nematic metal (NM), and a nematic insulator (NI). We have set $J = V = 1$ and the density to half-filling. The isotropic and nematic phases are separated by first-order or continuous thermal transitions which meet at a tricritical point (filled circle). The NM and NI regimes are separated by a crossover at nonzero T . (b) Temperature at the tricritical point versus δt showing that it could be potentially further tuned (see solid line, guide to eye) to reach a quantum tricritical point in a more generalized model. (c) Polarization (P), or orbital density imbalance for a cross section taken along the t - T plane in (a) with $\delta t/t = 0.05$. (d) Compressibility (κ), distinguishing metallic (SM and NM) from insulating phases, for a t - T plane cross section with $\delta t/t = 0.05$.

tricritical point can be tuned by the hopping anisotropy δt as shown in Fig. 2(b). We characterize the nematic order by the orbital polarization $P = \langle n_+ \rangle - \langle n_- \rangle$, where the orbital densities are computed as $\langle n_s \rangle = G_s(\tau = 0^-)$ or $\langle n_s \rangle = -\partial\Omega_s/\partial\mu$. As seen from Fig. 2(c), P increases sharply below the first-order transition, while it increases gradually below the continuous thermal transition. Everywhere in the nematic phase, the polarization remains below its maximal value $P_{\max} = 1$. These transitions also exhibit corresponding signatures in the entropy $S = -\partial\Omega/\partial T$ and the specific heat $C_v = T\partial S/\partial T$ (see supplemental material).

We next discuss the compressibility $\kappa = \langle n \rangle^{-2} \partial \langle n \rangle / \partial \mu$, where, $\langle n \rangle = \sum_s \langle n_s \rangle$ is the total number density of fermions which we set to half-filling. As seen in Fig. 2(d), the compressibility vanishes as $T \rightarrow 0$ at small t , but it remains nonzero at larger t . This allows us to distinguish insulating from metallic phases, which we also confirm below using spectral functions and transport. We observe that the nematic phase exhibits both metallic (NM) and insulating (NI) regimes; these appear to be separated by a continuous transition as $T \rightarrow 0$, and by

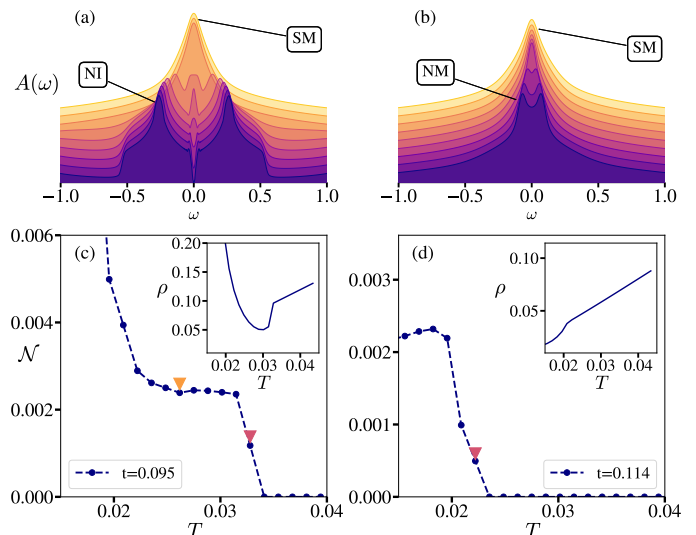


FIG. 3. (a) Evolution of the local spectral function $A(\omega)$ with temperature T as a function of frequency ω upon cooling from the isotropic SM into the NI. We find an intermediate window where nematicity coexists with a peak at $\omega = 0$ indicative of the NM. Upon cooling further, this peak converts into a gap, leading to the NI. (b) Same as (a) but for a regime where the $T \rightarrow 0$ phase is a NM, indicated by a finite-spectral weight at $\omega = 0$. (c) Resistive nematicity $\mathcal{N}(T)$ which is zero in the isotropic phase, increases (purple arrow) and saturates in the NM, and further rapidly increases (yellow arrow) at low T in the NI regime. Inset shows the average resistivity $\rho(T) = (\rho_{xx} + \rho_{yy})/2$. (d) Same as (c), but retains the NM state upon cooling. Inset indicates corresponding average resistivity $\rho(T)$. $\delta t/t = 0.05$ for all subfigures.

the indicated crossover lines in Fig. 2(a) at nonzero T .

Spectral functions. — To explore the spectral properties across the phase diagram, we have solved the analytically continued [51, 61] versions of the self-consistent equations 5 and 6 on the real frequency axis, from which we extract the local spectral function $A_s(\omega) = -\text{Im}G_s^{\text{ret}}(\omega)/\pi$. Here, $G_s^{\text{ret}}(\omega)$ is the retarded Green function obtained by analytically continuing $G_s(i\omega_n \rightarrow \omega^+)$.

Fig. 3 (a,b) shows the total spectral function $A(\omega) = \sum_s A_s(\omega)$ in the regimes where the $T = 0$ phase is (a) a nematic insulator and (b) a nematic metal respectively. At high T , both regimes feature an orbital symmetric strange metal regime with a peak at $\omega = 0$. Since orbital symmetry is broken below the nematic transition, the spectral functions for the two orbitals split and move away from $\omega = 0$, leading to twin peaks in $A(\omega)$, one from each orbital. Since $\langle n_s \rangle = \int_{-\infty}^{\infty} d\omega n_F(\omega) A_s(\omega)$, this splitting correlates with the onset of nonzero polarization P discussed earlier. Here, $n_F(\omega)$ denotes the Fermi function. The symmetries of the local spectral function in the isotropic phase, which include particle-hole symmetry, $A_s(\omega) = A_s(-\omega)$, and orbital-exchange symmetry, $A_s(\omega) = A_{-s}(\omega)$, get reduced in the nematic phase to a combined symmetry under $\omega \rightarrow -\omega$ followed by orbital exchange $s \rightarrow -s$, so that $A_s(\omega) = A_{-s}(-\omega)$.

From Fig. 3 (a), we find that there is a regime of temperatures below the nematic transition where a spectral peak survives at $\omega = 0$, suggestive of a NM, before a (soft) gap opens up leading to a loss of low frequency spectral weight, and eventually a hard insulating gap at $T = 0$. This is consistent with a vanishing compressibility $\kappa(T \rightarrow 0)$ for small values of hopping t in Fig. 2(d).

Transport. — Given the spectral functions above, the real part of the conductivity is most easily computed (along both directions $\alpha = x, y$) as

$$\text{Re}\sigma_{\alpha\alpha}(\omega, T) = \frac{1}{\omega} \sum_s \int_{\mathbf{k}, \omega'} v_{s,\alpha}^2(\mathbf{k}) A_s(\mathbf{k}, \omega') A_s(\mathbf{k}, \omega + \omega') \times [n_F(\omega') - n_F(\omega + \omega')], \quad (7)$$

where $\vec{v}_s(\mathbf{k}) = \vec{\nabla}_{\mathbf{k}} \varepsilon_s(\mathbf{k})$, and the momentum-resolved spectral function $A_s(\mathbf{k}, \omega) = -\text{Im} G_s(\mathbf{k}, \omega^+)/\pi$ is obtained from the lattice Green's function $G_s(\mathbf{k}, \omega^+) = 1/(\omega^+ + \mu - \varepsilon_s(\mathbf{k}) - \sum_n (i\omega_n \rightarrow \omega^+))$.

In the $N \rightarrow \infty$ limit, this disorder averaged Kubo formula result has been shown to be exact, with no vertex corrections [69, 70], and with a separable product of disorder averaged Green functions $\overline{GG} = \overline{G} \overline{G}$ [64]. We extract the d.c. conductivity as the slope of the $\omega\sigma_{\alpha\alpha}(\omega)$ curve for $\omega \rightarrow 0$, and invert it to obtain the d.c. resistivity $\rho_{\alpha\alpha}$. Fig. 3(c) and (d) show the *resistive nematicity* $\mathcal{N} = (\rho_{xx} - \rho_{yy})/(\rho_{xx} + \rho_{yy})$ as a function of temperature, with the average resistivity plotted in the corresponding insets. The nematic metal which emerges from the high temperature strange metal regime is a Fermi liquid with $\rho_{\alpha\alpha} \propto T^2$. We find that $\mathcal{N}(T)$ vanishes in the isotropic phase, while it displays a plateau in the NM, before rapidly increasing to $\mathcal{N} \sim \mathcal{O}(1)$ deep in the NI.

Elastotransport. — It has been shown that transport in the presence of uniaxial strain can provide a sensitive probe of nematic fluctuations and the onset of nematic order [43, 46]. In order to explore this, we assume that the uniaxial strain imposes a local orbital splitting which varies linearly with the strain; physically, this will arise due to a modification in the local crystal field environment. Given its strain-induced origin, we use ϵ to denote this splitting. This leads to an additional term in the Hamiltonian $\epsilon \sum_{\mathbf{r}} (n_{\mathbf{r},+,i} - n_{\mathbf{r},-,i})$. To explore the impact of strain on transport, we solve the self-consistent large- N equations with a nonzero ϵ and compute changes in the resistivity $\delta\rho_{\alpha\alpha}$. Fig. 4(a) shows the computed differential anisotropic elastoresistivity $\mathcal{N}_\epsilon(T) = (\delta\rho_{xx} - \delta\rho_{yy})/\epsilon$ for different hoppings t , corresponding to different cuts through the phase diagram which pass through the nematic metal. Here $\delta\rho_{\alpha\alpha}$ represents the change in resistivity from its unstrained value due to a weak nonzero $\epsilon = 10^{-3}$. We find that $\mathcal{N}_\epsilon(T)$ shows a significant increase upon cooling towards the nematic transition, with a peak at the onset of nematic order. In this particle-hole symmetric model, we expect \mathcal{N}_ϵ to be dominated by changes in the orbital occupation rather than inducing orbital-dependent scattering rates, so that \mathcal{N}_ϵ reflects changes in the orbital polarization due to strain is thus

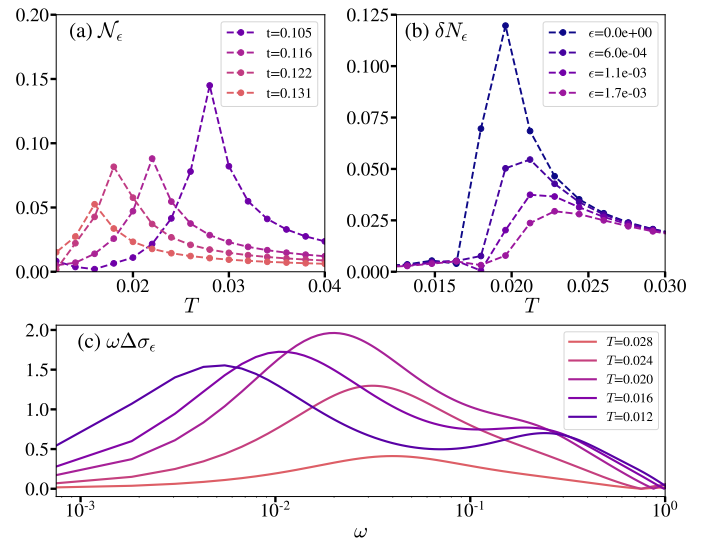


FIG. 4. $\mathcal{N}_\epsilon(T) = (\delta\rho_{xx} - \delta\rho_{yy})/\epsilon$ is the anisotropic differential elastoresistivity (see text for details) for $\epsilon = 10^{-3}$, for various cuts through the SM-NM transition; the peaks correspond to T_c . (b) Strain dependence of $\delta\mathcal{N}_\epsilon(T)$ for $t = 0.12$ showing that the transition and hence $\delta\mathcal{N}_\epsilon(T)$ gets rounded with increasing strain. (c) $\omega\Delta\sigma_\epsilon(\omega)$ versus frequency for $t = 0.12$, where $\omega\Delta\sigma_\epsilon(\omega)$ is the anisotropic differential elastoconductivity, at fixed small strain $\epsilon = 10^{-3}$. Here, $\delta t/t = 0.05$ for all subfigures.

tied to the nematic susceptibility. Fig. 4(b) shows the strain dependence of the differential anisotropic elastoresistivity $\delta\mathcal{N}_\epsilon(T)$ for a fixed hopping t , where we compute the resistivity $\delta\rho_{\alpha\alpha}$ at two nearby strain values ϵ (indicated in the plot) and $\epsilon + d\epsilon$ with $d\epsilon = 10^{-4}$. We see that with increasing ϵ , which imposes orbital symmetry breaking, the nematic phase transition gets rounded out.

We finally turn to the frequency-dependent elastoconductivity for weak nonzero strain. Fig. 4(c) shows plots of $\omega\Delta\sigma_\epsilon(\omega)$ as a function of temperature as we cool into the nematic insulator, where $\Delta\sigma_\epsilon(\omega) = \text{Re}(\delta\sigma_{xx} - \delta\sigma_{yy})/\epsilon$ is the differential anisotropic elastoconductivity obtained from the change in conductivities due to $\epsilon = 10^{-3}$. We find that $\omega\Delta\sigma_\epsilon(\omega)$ exhibits a bump near $\omega \sim 0.03$ (at higher T), which shifts to lower frequency upon cooling, and is largest near T_c . We expect the location of this peak to track the scattering rate, with the peak height tracking the nematic susceptibility. Indeed, in a simple Drude-like theory, with $\text{Re}\sigma(\omega) = (ne^2\tau/m)/(1 + \omega^2\tau^2)$, there is a peak of $\omega\Delta\sigma(\omega)$ at $\omega = 1/\tau$, with the peak height $ne^2/2m$. It is thus plausible that the peak in $\omega\Delta\sigma_\epsilon(\omega)$ could be a better measure of the nematic susceptibility, being independent of the scattering rate even in a more general setting where particle-hole symmetry is lost. The second peak in $\omega\Delta\sigma(\omega)$, visible at higher frequency, reflects subtle features in the single-particle spectrum.

Summary. — We have proposed a two-orbital model for a nFL which undergoes a $C_4 \rightarrow C_2$ rotational

symmetry-breaking transition to a nematic phase, and studied its thermodynamic and transport properties. Our work opens up a new avenue to exploring the interplay of nematicity and nFL physics with possible implications for diverse experimental systems. In future, it would be interesting to explore the fate of nematic phases and phase transitions if the SYK couplings in our model are made translationally invariant at the Hamilto-

nian level, leading to momentum dependent self energies.

We thank Anjishnu Bose for discussions. We acknowledge support from the Natural Sciences and Engineering Research Council (NSERC) of Canada. A. Hardy acknowledges funding from the Canada Graduate Scholarship (NSERC). Numerical computations were performed on the Niagara supercomputer at the SciNet HPC Consortium and Compute Canada.

-
- [1] A. J. Millis, Effect of a nonzero temperature on quantum critical points in itinerant fermion systems, *Physical Review B* **48**, 7183 (1993).
- [2] G. R. Stewart, Non-Fermi-liquid behavior in d - and f - electron metals, *Reviews of Modern Physics* **73**, 797 (2001).
- [3] C. Varma, Z. Nussinov, and W. van Saarloos, Singular or non-fermi liquids, *Physics Reports* **361**, 267417 (2002).
- [4] M. J. Lawler, D. G. Barci, V. Fernández, E. Fradkin, and L. Oxman, Nonperturbative behavior of the quantum phase transition to a nematic Fermi fluid, *Physical Review B - Condensed Matter and Materials Physics* **73**, 1 (2006), arXiv:0508747 [cond-mat].
- [5] M. A. Metlitski and S. Sachdev, Quantum phase transitions of metals in two spatial dimensions. I. Ising-nematic order, *Physical Review B - Condensed Matter and Materials Physics* **82**, 41 (2010), arXiv:1001.1153.
- [6] S.-S. Lee, Recent Developments in Non-Fermi Liquid Theory, *Annual Review of Condensed Matter Physics*, 20 (2018).
- [7] C. M. Varma, Colloquium : Linear in temperature resistivity and associated mysteries including high temperature superconductivity, *Reviews of Modern Physics* **92**, 10.1103/revmodphys.92.031001 (2020).
- [8] A. V. Chubukov, C. Pépin, and J. Rech, Instability of the quantum-critical point of itinerant ferromagnets, *Physical Review Letters* **92**, 147003 (2004).
- [9] U. Karahasanovic, F. Krger, and A. G. Green, Quantum order-by-disorder driven phase reconstruction in the vicinity of ferromagnetic quantum critical points, *Physical Review B* **85**, 10.1103/physrevb.85.165111 (2012).
- [10] E. Berg, M. A. Metlitski, and S. Sachdev, Sign-problem-free quantum monte carlo of the onset of antiferromagnetism in metals, *Science* **338**, 16061609 (2012).
- [11] J. A. Damia, S. Kachru, S. Raghu, and G. Torroba, Two-dimensional non-fermi-liquid metals: A solvable large- n limit, *Physical Review Letters* **123**, 10.1103/physrevlett.123.096402 (2019).
- [12] E. Berg, S. Lederer, Y. Schattner, and S. Trebst, Monte Carlo Studies of Quantum Critical Metals, *Annual Review of Condensed Matter Physics* **10**, 63 (2019).
- [13] A. Abanov, Y.-M. Wu, Y. Wang, and A. V. Chubukov, Superconductivity above a quantum critical point in a metal: Gap closing versus gap filling, fermi arcs, and pseudogap behavior, *Physical Review B* **99**, 10.1103/physrevb.99.180506 (2019).
- [14] Y. Cao, D. Rodan-Legrain, J. M. Park, N. F. Q. Yuan, K. Watanabe, T. Taniguchi, R. M. Fernandes, L. Fu, and P. Jarillo-Herrero, Nematicity and competing orders in superconducting magic-angle graphene, *Science* **372**, 264 (2014).
- [15] Y. Cao, D. Chowdhury, D. Rodan-Legrain, O. Rubies-Bigorda, K. Watanabe, T. Taniguchi, T. Senthil, and P. Jarillo-Herrero, Strange metal in magic-angle graphene with near planckian dissipation, *Physical Review Letters* **124**, 076801 (2020).
- [16] C. Rubio-Verd, S. Turkel, Y. Song, L. Klebl, R. Samajdar, M. S. Scheurer, J. W. F. Venderbos, K. Watanabe, T. Taniguchi, H. Ochoa, L. Xian, D. M. Kennes, R. M. Fernandes, C. Rubio, and A. N. Pasupathy, Moiré nematic phase in twisted double bilayer graphene, *Nature Physics* **18**, 196 (2022).
- [17] R. M. Fernandes, A. V. Chubukov, J. Knolle, I. Eremin, and J. Schmalian, Preemptive nematic order, pseudogap, and orbital order in the iron pnictides, *Physical Review B* **85**, 024534 (2012).
- [18] S. Avci, O. Chmaissem, J. Allred, S. Rosenkranz, I. Eremin, A. Chubukov, D. Bugaris, D. Chung, M. Kanatzidis, J.-P. Castellan, J. Schlueter, H. Claus, D. Khalavin, P. Manuel, A. Daoud-Aladine, and R. Osborn, Magnetically driven suppression of nematic order in an iron-based superconductor, *Nature Communications* **5**, 3845 (2014).
- [19] R. M. Fernandes, A. V. Chubukov, and J. Schmalian, What drives nematic order in iron-based superconductors?, *Nature Physics* **10**, 97 (2014).
- [20] J. K. Glasbrenner, I. I. Mazin, H. O. Jeschke, P. J. Hirschfeld, R. M. Fernandes, and R. Valent, Effect of magnetic frustration on nematicity and superconductivity in iron chalcogenides, *Nature Physics* **11**, 953958 (2015).
- [21] P. O. Sprau, A. Kostin, A. Kreisel, A. E. Böhmer, V. Taufour, P. C. Canfield, S. Mukherjee, P. J. Hirschfeld, B. M. Andersen, and J. C. S. Davis, Discovery of orbital-selective cooper pairing in fese, *Science* **357**, 7580 (2017).
- [22] R. Khasanov, R. M. Fernandes, G. Simutis, Z. Guguchia, A. Amato, H. Luetkens, E. Morenzoni, X. Dong, F. Zhou, and Z. Zhao, Magnetic tricritical point and nematicity in FeSe under pressure, *Physical Review B* **97**, 224510 (2018).
- [23] S. Licciardello, J. Buhot, J. Lu, J. Ayres, S. Kasahara, Y. Matsuda, T. Shibauchi, and N. E. Hussey, Electrical resistivity across a nematic quantum critical point, *Nature* **567**, 213 (2019).
- [24] M. Culo, M. Berben, Y.-T. Hsu, J. Ayres, R. D. H. Hinlopen, S. Kasahara, Y. Matsuda, T. Shibauchi, and N. E. Hussey, Putative Hall response of the strange metal component in Fe Se_{1-x}S_x, *Physical Review Research* **3**, 023069 (2021).
- [25] D. Steffensen, A. Kreisel, P. J. Hirschfeld, and B. M. Andersen, Interorbital nematicity and the origin of a single electron fermi pocket in fese, *Physical Review B* **103**,

- 10.1103/physrevb.103.054505 (2021).
- [26] L. Nie, A. V. Maharaj, E. Fradkin, and S. A. Kivelson, Vestigial nematicity from spin and/or charge order in the cuprates, *Physical Review B* **96**, 085142 (2017).
- [27] S. Mukhopadhyay, R. Sharma, C. K. Kim, S. D. Edkins, M. H. Hamidian, H. Eisaki, S.-i. Uchida, E.-A. Kim, M. J. Lawler, A. P. Mackenzie, J. C. S. Davis, and K. Fujita, Evidence for a vestigial nematic state in the cuprate pseudogap phase, *Proceedings of the National Academy of Sciences* **116**, 13249 (2019).
- [28] N. K. Gupta, C. McMahon, R. Sutarto, T. Shi, R. Gong, H. I. Wei, K. M. Shen, F. He, Q. Ma, M. Dragomir, B. D. Gaulin, and D. G. Hawthorn, Vanishing nematic order beyond the pseudogap phase in overdoped cuprate superconductors, *Proceedings of the National Academy of Sciences* **118**, e2106881118 (2021).
- [29] R. A. Borzi, S. A. Grigera, J. Farrell, R. S. Perry, S. J. S. Lister, S. L. Lee, D. A. Tennant, Y. Maeno, and A. P. Mackenzie, Formation of a nematic fluid at high fields in $\text{Sr}_3\text{Ru}_2\text{O}_7$, *Science* **315**, 214217 (2007).
- [30] I. Khavkine, C.-H. Chung, V. Oganesyan, and H.-Y. Kee, Formation of an electronic nematic phase in interacting fermion systems, *Physical Review B* **70**, 10.1103/physrevb.70.155110 (2004).
- [31] H.-Y. Kee and Y. B. Kim, Itinerant metamagnetism induced by electronic nematic order, *Physical Review B* **71**, 10.1103/physrevb.71.184402 (2005).
- [32] S. Raghu, A. Paramekanti, E. A. Kim, R. A. Borzi, S. A. Grigera, A. P. Mackenzie, and S. A. Kivelson, Microscopic theory of the nematic phase in $\text{Sr}_3\text{Ru}_2\text{O}_7$, *Physical Review B* **79**, 10.1103/physrevb.79.214402 (2009).
- [33] C. M. Puetter, S. D. Swiecicki, and H.-Y. Kee, Unveiling a nematic quantum critical point in multi-orbital systems, *New Journal of Physics* **14**, 053027 (2012).
- [34] C. Lester, S. Ramos, R. S. Perry, T. P. Croft, R. I. Bewley, T. Guidi, P. Manuel, D. D. Khalyavin, E. Forgan, and S. M. Hayden, Field-tunable spin-density-wave phases in $\text{Sr}_3\text{Ru}_2\text{O}_7$, *Nature Materials* **14**, 373378 (2015).
- [35] K. B. Cooper, M. P. Lilly, J. P. Eisenstein, L. N. Pfeiffer, and K. W. West, Onset of anisotropic transport of two-dimensional electrons in high Landau levels: Possible isotropic-to-nematic liquid-crystal phase transition, *Physical Review B* **65**, 10.1103/physrevb.65.241313 (2002).
- [36] E. Fradkin, S. A. Kivelson, M. J. Lawler, J. P. Eisenstein, and A. P. Mackenzie, Nematic fermi fluids in condensed matter physics, *Annual Review of Condensed Matter Physics* **1**, 153 (2010), arXiv:0910.4166.
- [37] B. E. Feldman, M. T. Randeria, A. Gyenis, F. Wu, H. Ji, R. J. Cava, A. H. MacDonald, and A. Yazdani, Observation of a nematic quantum Hall liquid on the surface of Bismuth, *Science* **354** (2016).
- [38] I. M. Hayes, N. Maksimovic, G. N. Lopez, M. K. Chan, B. J. Ramshaw, R. D. McDonald, and J. G. Analytis, Superconductivity and quantum criticality linked by the Hall effect in a strange metal, *Nature Physics* **17**, 58 (2021).
- [39] H. Ikeda, M. T. Suzuki, R. Arita, T. Takimoto, T. Shibauchi, and Y. Matsuda, Emergent rank-5 nematic order in URu_2Si_2 , *Nature Physics* **8**, 528 (2012), arXiv:1204.4016.
- [40] J. Xia, J. P. Eisenstein, L. N. Pfeiffer, and K. W. West, Evidence for a fractionally quantized Hall state with anisotropic longitudinal transport, *Nature Physics* **7**, 845 (2011).
- [41] Y. Schattner, S. Lederer, S. A. Kivelson, and E. Berg, Ising nematic quantum critical point in a metal: A monte carlo study, *Physical Review X* **6**, 031028 (2016).
- [42] H.-H. Kuo, M. C. Shapiro, S. C. Riggs, and I. R. Fisher, Measurement of the elastoresistivity coefficients of the underdoped iron arsenide $\text{Ba}(\text{Fe}_{0.975}\text{Co}_{0.025})_2\text{As}_2$, *Physical Review B* **88**, 085113 (2013).
- [43] C. Mirri, A. Dusza, S. Bastelberger, M. Chinotti, J.-H. Chu, H.-H. Kuo, I. R. Fisher, and L. Degiorgi, Electrodynamic response in the electronic nematic phase of BaFe_2As_2 , *Physical Review B* **93**, 085114 (2016).
- [44] J. C. Palmstrom, P. Walmsley, J. A. W. Straquadine, M. E. Sorensen, S. T. Hannahs, D. H. Burns, and I. R. Fisher, Comparison of temperature and doping dependence of elastoresistivity near a putative nematic quantum critical point, *Nature Communications* **13**, 1011 (2022).
- [45] J. M. Bartlett, A. Steppke, S. Hosoi, H. Noad, J. Park, C. Timm, T. Shibauchi, A. P. Mackenzie, and C. W. Hicks, Relationship between transport anisotropy and nematicity in FeSe, *Physical Review X* **11**, 10.1103/physrevx.11.021038 (2021).
- [46] M. Arciniaga, P. Mai, and B. S. Shastry, Theory of anisotropic elastoresistivity of two-dimensional extremely strongly correlated metals, *Physical Review B* **101**, 245149 (2020).
- [47] S. Sachdev and J. Ye, Gapless spin-fluid ground state in a random quantum Heisenberg magnet, *Physical Review Letters* **70**, 3339 (1993).
- [48] S. Sachdev, Holographic Metals and the Fractionalized Fermi Liquid, *Phys. Rev. Lett.* **105**, 151602 (2010).
- [49] A. Kitaev, A simple model of quantum holography, *Talks at KITP, April 7, 2015 and May 27, 2015* (2015).
- [50] J. Maldacena and D. Stanford, Remarks on the Sachdev-Ye-Kitaev model, *Phys. Rev. D* **94**, 106002 (2016).
- [51] S. Banerjee and E. Altman, Solvable model for a dynamical quantum phase transition from fast to slow scrambling, *Physical Review B* **95**, 134302 (2017).
- [52] A. Haldar and V. B. Shenoy, Strange half-metals and Mott insulators in Sachdev-Ye-Kitaev models, *Physical Review B* **98**, 165135 (2018).
- [53] J. Kim, X. Cao, and E. Altman, Low-rank Sachdev-Ye-Kitaev models, *Physical Review B* **101**, 125112 (2020).
- [54] I. Esterlis and J. Schmalian, Cooper pairing of incoherent electrons: An electron-phonon version of the Sachdev-Ye-Kitaev model, *Physical Review B* **100**, 115132 (2019).
- [55] Y. Wang, Solvable Strong-Coupling Quantum-Dot Model with a Non-Fermi-Liquid Pairing Transition, *Physical Review Letters* **124**, 017002 (2020).
- [56] Y. Wang and A. V. Chubukov, Quantum phase transition in the Yukawa-SYK model, *Physical Review Research* **2**, 10.1103/physrevresearch.2.033084 (2020).
- [57] É. Lantagne-Hurtubise, V. Pathak, S. Sahoo, and M. Franz, Superconducting instabilities in a spinful Sachdev-Ye-Kitaev model, *Physical Review B* **104**, L020509 (2021).
- [58] D. Chowdhury, A. Georges, O. Parcollet, and S. Sachdev, Sachdev-Ye-Kitaev Models and Beyond: A Window into Non-Fermi Liquids, arXiv:2109.05037 (2021), arXiv:2109.05037.
- [59] L. Classen and A. Chubukov, Superconductivity of incoherent electrons in the Yukawa Sachdev-Ye-

- Kitaev model, *Physical Review B* **104**, [10.1103/physrevb.104.125120](#) (2021).
- [60] Y. Gu, X.-L. Qi, and D. Stanford, Local criticality, diffusion and chaos in generalized Sachdev-Ye-Kitaev models, *Journal of High Energy Physics* **2017**, 1 (2017).
- [61] A. Haldar, S. Banerjee, and V. B. Shenoy, Higher-dimensional Sachdev-Ye-Kitaev non-Fermi liquids at Lifshitz transitions, *Physical Review B* **97**, 1 (2018).
- [62] X. Y. Song, C. M. Jian, and L. Balents, Strongly Correlated Metal Built from Sachdev-Ye-Kitaev Models, *Physical Review Letters* **119**, 1 (2017), [arXiv:1705.00117](#).
- [63] P. Zhang, Dispersive Sachdev-Ye-Kitaev model: Band structure and quantum chaos, *Physical Review B* **96**, 205138 (2017).
- [64] D. Chowdhury, Y. Werman, E. Berg, and T. Senthil, Translationally invariant non-fermi-liquid metals with critical fermi surfaces: Solvable models, *Phys. Rev. X* **8**, 031024 (2018).
- [65] C.-M. Jian, Z. Bi, and C. Xu, Model for continuous thermal metal to insulator transition, *Physical Review B* **96**, 115122 (2017).
- [66] E. E. Aldape, T. Cookmeyer, A. A. Patel, and E. Altman, Solvable Theory of a Strange Metal at the Breakdown of a Heavy Fermi Liquid, [arXiv:2012.00763](#) (2022), [arXiv:2012.00763](#).
- [67] I. Esterlis, H. Guo, A. A. Patel, and S. Sachdev, Large- n theory of critical fermi surfaces, *Physical Review B* **103**, 235129 (2021).
- [68] A. Haldar, O. Tavakol, and T. Scaffidi, Variational wave functions for Sachdev-Ye-Kitaev models, *Phys. Rev. Research* **3**, 023020 (2021).
- [69] A. A. Patel and S. Sachdev, Theory of a Planckian metal, *Physical Review Letters* **123**, 066601 (2019), [arXiv:1906.03265](#).
- [70] G. Jose, K. Seo, and B. Uchoa, Non-Fermi liquid behavior in the Sachdev-Ye-Kitaev model for a one dimensional incoherent semimetal, [arXiv:2103.12110](#) (2022), [arXiv:2103.12110](#).